Formation of He* by ion–ion neutralization reactions of He + with C 6 F 5 X − (X=F, Cl, Br, CF 3) in a helium flowing afterglow

Masaharu Tsuji, Masafumi Nakamura, Yukio Nishimura, Erika Oda, Hidefumi Oota, and Masahiro Hisano

Citation: The Journal of Chemical Physics **110**, 2903 (1999); doi: 10.1063/1.477933
View online: http://dx.doi.org/10.1063/1.477933
View Table of Contents: http://scitation.aip.org/content/aip/journal/jcp/110/6?ver=pdfcov
Published by the AIP Publishing

Formation of He* by ion–ion neutralization reactions of He^+ with $C_6F_5X^-$ (X=F, Cl, Br, CF_3) in a helium flowing afterglow

Masaharu Tsuji, Masafumi Nakamura, and Yukio Nishimura
Institute of Advanced Material Study, Kyushu University, Kasuga-shi, Fukuoka 816-8580, Japan

Erika Oda
Department of Molecular Science and Technology, Graduate School of Engineering Sciences, Kyushu University, Kasuga-shi, Fukuoka, 816-8580, Japan

Hidefumi Oota and Masahiro Hisano
Department of Applied Science of Electronics and Materials, Graduate School of Engineering Sciences, Kyushu University, Kasuga-shi, Fukuoka 816-8580, Japan

(Received 4 August 1998; accepted 3 November 1998)

The ion–ion neutralization reactions of He^+ with $C_6F_5X^-$ (X=F, Cl, Br, CF_3) leading to He* have been spectroscopically studied in a helium flowing afterglow. Although both singlet and triplet He* states were formed when X=F and Cl, only triplet He* states were produced when X=Br and CF_3. More than 99% of the product He* atoms were formed in the low-lying He($3s$, $3p$, or $3d$) states for all the reactions, and their electronic-state distributions were similar. The electronic-state populations decreased rapidly with increasing excitation energy of He*. They were represented by effective electronic temperatures of 0.070–0.19 eV. The observed electronic-state distributions were compared with those predicted from a simple statistical theory. © *1999 American Institute of Physics.* [S0021-9606(99)00706-0]

I. INTRODUCTION

Although electron–ion and ion–ion recombination processes contribute significantly to the loss of charged species from cold plasmas, little information on the product-state distribution has been obtained.[1] We have recently succeeded in applying a flowing–afterglow method to optical spectroscopic studies of electron–ion and ion–ion recombination processes.[2–12] Very recently, we have studied the formation of He* in a helium flowing afterglow.[7] Fifty-one singlet and triplet ns, np, and nd Rydberg states of He* in the 22.72–24.53 eV range were identified as produced by electron–ion recombination processes. The dependence of the emission intensities on the He pressure and the electron density indicated that these He* states were formed by the three-body collisional radiative recombination reaction,

$$He^+ + e^- + e^- \rightarrow He^* + e^-, \tag{1}$$

where an electron acts as a third body. The excited electronic-state distributions, which were independent of He pressure in the 1.0–2.7 Torr range, increased with decreasing excitation energy of He*. They were expressed by double Boltzmann distributions with effective electronic temperatures of 0.46 eV in the 22.7–24.4 eV range and 0.089 eV in the 24.4–24.5 eV range. The low-temperature component at the high-energy range was explained by the Saha equilibrium between He* and free electrons, while the high-energy component at the low-energy range was discussed in terms of the non-Saha equilibrium due to the collisional excitation to a neighboring state and low reionization rates. The total steady-state distributions of $ns\,^1S$, $np\,^1P$, $nd\,^1D$, $ns\,^3S$, $np\,^3P$, and $nd\,^3D$ states are 0.22, 0.079, 0.17, 0.36, 0.066, and 0.10, respectively. The observed electronic-state distributions did not agree with that predicted from simple statistical theory, when a long-lived $[He^+ - e^-]$ was assumed.

In the present study, ion–ion neutralization reactions of He^+ with $C_6F_5X^-$ (X=F, Cl, Br, CF_3) leading to He* have been spectroscopically studied in the helium flowing afterglow. The electronic-state distributions are determined and compared with those predicted from a simple statistical theory in order to obtain dynamical features of the neutralization processes. Preliminary results for the $He^+/C_6F_6^-$ reaction have been communicated previously.[5]

II. EXPERIMENT

The flowing-afterglow apparatus used in this study was similar to that reported previously.[3,13] A schematic diagram of the flowing afterglow used for studying ion–ion neutralization reactions is shown in Fig. 1. It consists of a stainless steel main flow tube and a quartz discharge tube in which He($2\,^3S$), He^+, and electrons were produced by a microwave discharge in high purity He gas. Although a reagent C_6F_5X gas was injected from the first or second gas inlet located 10 and 20 cm downstream from the center of the discharge, respectively, the latter case is shown in Fig. 1. There are two regions in the helium flowing afterglow above and below the inlet of C_6F_5X. They are denoted by regions A and B in Fig. 1, respectively. Active species in region A were He($2\,^3S$), He^+, and electrons formed directly in the discharge region, and He_2^+ formed by the secondary ionic reaction

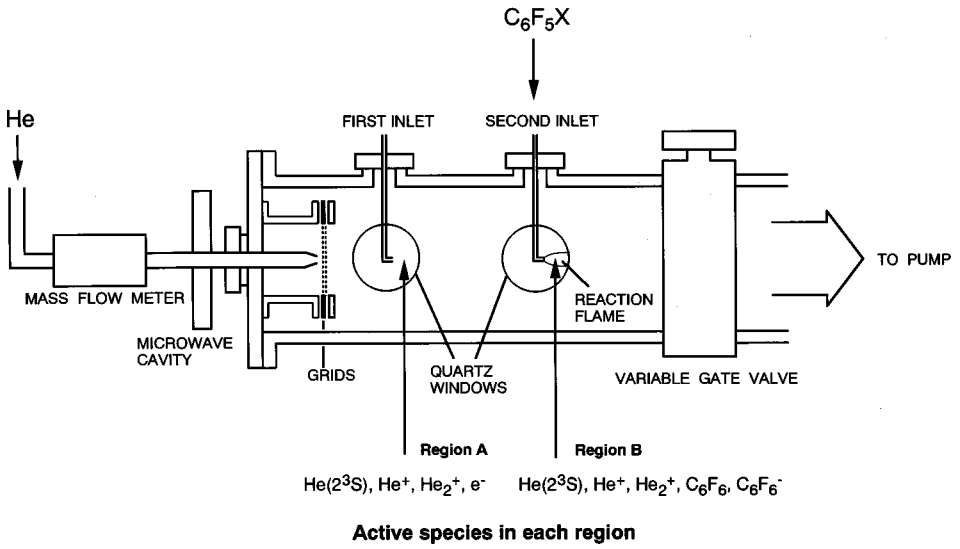

FIG. 1. Schematic diagram of the flowing afterglow for studying ion–ion neutralization reactions between He^+ and $C_6F_5X^-$.

$$He^+ + 2He \rightarrow He_2^+ + He, \quad (2)$$

$$k_2 = 8.3\times10^{-32}\ \text{cm}^6\,\text{molecule}^{-2}\,\text{s}^{-1}\ \text{(Ref. 14)}.$$

In region B, the $C_6F_5X^-$ (X=F, Cl, Br, CF_3) anions were formed by a fast electron attachment to C_6F_5X,

$$e^- + C_6F_6 \rightarrow C_6F_6^- \quad (100\%), \quad (3)$$

$$k_3 = 2.1\times10^{-7}\ \text{cm}^3\,\text{s}^{-1}\ \text{(Refs. 15, 16)},$$

$$e^- + C_6F_5Cl \rightarrow C_6F_5Cl^- \quad (100\%), \quad (4)$$

$$k_4 = 8.4\times10^{-8}\ \text{cm}^3\,\text{s}^{-1}\ \text{(Ref. 17)},$$

$$e^- + C_6F_5Br \rightarrow C_6F_5Br^- \quad (\geqslant 97\%) \quad (5a)$$

$$\rightarrow Br^- + C_6F_5 \quad (\leqslant 3\%), \quad (5b)$$

$$k_{5a} + k_{5b} = 8.3\times10^{-8}\ \text{cm}^3\,\text{s}^{-1}\ \text{(Ref. 17)},$$

$$e^- + C_6F_5CF_3 \rightarrow C_6F_5CF_3^-, \quad (6)$$

$$k_6 = 2.42\times10^{-7}\ \text{cm}^3\,\text{s}^{-1}\ \text{(Refs. 15,18)}.$$

Thus, the active species in region B were $He(2\,^3S)$, He^+, He_2^+, C_6F_5X, and $C_6F_5X^-$. The partial pressure in the reaction zone was 0.6–2.5 Torr for He and 1–10 mTorr for C_6F_5X. The electron density, $[e^-]$, was measured using a single Langmuir probe. The $[e^-]$ value was determined to be $3.2\times10^9 - 2.6\times10^{10}\,\text{cm}^{-3}$ in a He pressure range of 0.2–1.4 Torr using the same procedure as that reported by Smith *et al.*[19,20] Since thermal electrons were completely scavenged through processes (3)–(6), the density of $C_6F_5X^-$ was expected to be nearly the same as that of the electron density.

Emission spectra from region B were dispersed in the 200–840 nm region with a Spex 1250 M monochromator. Digital photon signals from a cooled photomultiplier were stored and analyzed with a microcomputer. The relative sensitivity of the monochromator and photomultiplier was calibrated using standard D_2 and halogen lamps. The contribution of He^+ and He_2^+ ions to the observed emissions was examined using a pair of ion-collector grids placed on an exit opening of the discharge tube.

III. RESULTS AND DISCUSSION

A. Excitation process of He* in a helium flowing afterglow

When the emission spectrum from a He afterglow was observed without the addition of C_6F_5X (X=F, Cl, Br, or CF_3), 51 He* lines due to $He^+/2e^-$ collisional-radiative recombination (1) were observed in the 260–1000 nm region.[7] They were ascribed to the following six Rydberg series of He* lines with excitation energies of 22.72–24.53 eV[21]: $ns\,^1S \rightarrow 2p\,^1P(n=3-6)$, $ns\,^3S \rightarrow 2p\,^3P(n=3-8)$, $np\,^1P \rightarrow 2s\,^1S(n=3-10)$, $np\,^3P \rightarrow 2s\,^3S(n=3-13)$, $nd\,^1D \rightarrow 2p\,^1P(n=3-10)$, and $nd\,^3D \rightarrow 2p\,^3P(n=3-16)$. By the addition of C_6F_5X into the He afterglow, almost all He* lines with high excitation energies above 24 eV disappeared, and only 2–8 lines with low excitation energies are observed. These results indicate that electrons are completely scavenged by C_6F_5X, so that the contribution of the $He^+/2e^-$ reaction to the formation of He* is negligible.

For example, Fig. 2(a) shows a typical emission spectrum observed by the addition of C_6F_5Cl into the helium afterglow, where several He* lines and a broad $C_6F_5Cl^+(\tilde{B}-\tilde{X})$ band in the 470–650 nm region[22] are observed. When He^+ and He_2^+ are trapped using the ion-collector grids, some He* lines and the $C_6F_5Cl^+(\tilde{B}-\tilde{X})$ band reduce their intensities, as shown in Fig. 2(b). These results imply that He^+ and/or He_2^+ take part in the formation of these emissions. The He* lines observed in Fig. 2(b) are stray He* emissions resulting from the microwave discharge of He. On the other hand, the $C_6F_5Cl^+(\tilde{B}-\tilde{X})$ band in Fig. 2(b) arises from the $He(2\,^3S)/C_6F_5Cl$ Penning ionization,

$$He(2\,^3S) + C_6F_5Cl \rightarrow C_6F_5Cl^+(\tilde{B}) + He + e^-. \quad (7)$$

Although process (7) becomes an additional source of electrons, Penning electrons are rapidly scavenged by C_6F_5Cl through process (4). The dependence of the emission intensity of the $C_6F_5Cl^+(\tilde{B}-\tilde{X})$ band resulting from ionic reaction was similar to that of the $CO_2^+(\tilde{B}-\tilde{X})$ emission resulting from the He_2^+/CO_2 charge-transfer reaction.[23] Therefore, the

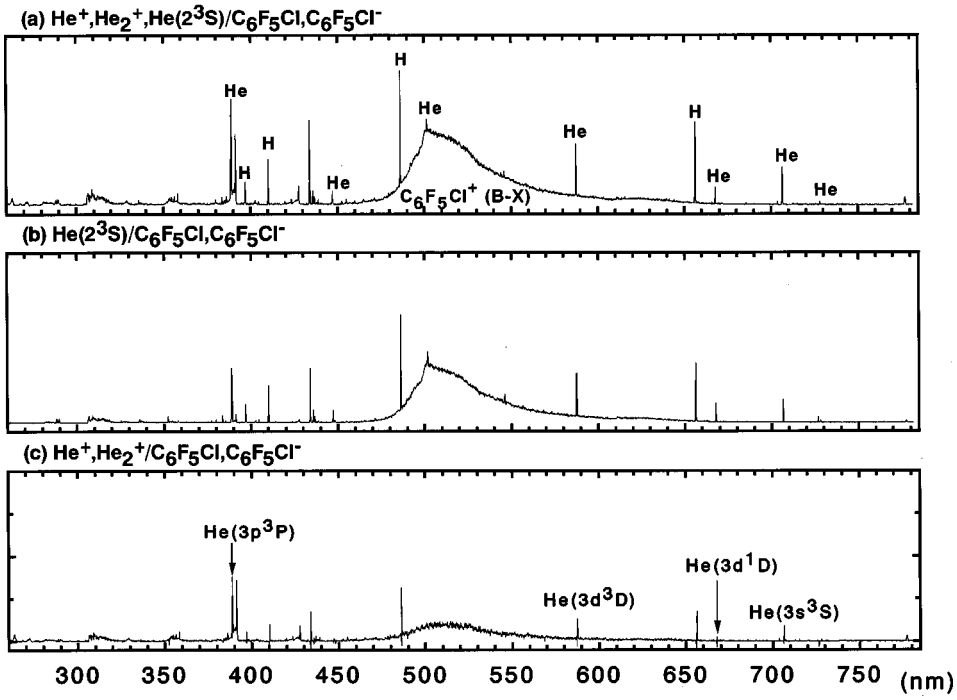

FIG. 2. Emission spectra observed by the addition of C_6F_5Cl into a He flowing afterglow. Helium active species in (a) are $He(2\,^3S)$, He^+, and He_2^+ and (b) are $He\,(2\,^3S)$, and (c) is a difference spectrum between (a) and (b) [(a)–(b)]. $OH(A-X$: ~310 nm) and H (Balmer series) bands due to H_2O impurity are also observed.

He_2^+/C_6F_5Cl reaction was concluded to be responsible for the $C_6F_5Cl^+(\tilde{B}-\tilde{X})$ emission resulting from ionic reaction,

$$He_2^+ + C_6F_5Cl \rightarrow C_6F_5Cl^+(\tilde{B}) + 2He. \quad (8)$$

The emission spectrum resulting from ionic reactions was obtained by subtracting Fig. 2(b) from Fig. 2(a). The result obtained is shown in Fig. 2(c), where besides a weak $C_6F_5Cl^+(\tilde{B}-\tilde{X})$ emission due to process (8), a few He* lines, on which the present study is focused, are found. The He^+ and/or He_2^+ ions are responsible for the formation of the He* lines in Fig. 2(c). Therefore, possible excitation processes of He* are the following charge-transfer and ion–ion neutralization reactions:

$$He^+ + C_6F_5X \rightarrow He^* + C_6F_5X^+, \quad (9)$$

$$He_2^+ + C_6F_5X \rightarrow He^* + He + C_6F_5X^+, \quad (10)$$

$$He^+ + C_6F_5X^- \rightarrow He^* + C_6F_5X, \quad (11)$$

$$He^+ + C_6F_5X^- \rightarrow He^* + C_6F_5 + X, \quad (12)$$

$$He_2^+ + C_6F_5X^- \rightarrow He^* + He + C_6F_5X. \quad (13)$$

Charge-transfer reactions (9) and (10) are highly endoergic ($\Delta H > 10$ eV) on the basis of reported thermochemical data.[21,24–26] Ion–ion neutralization processes (12) and (13) are also endoergic ($\Delta H = 1.0–3.9$ eV) on the basis of reported thermochemical and spectroscopic data.[21,24–26] Therefore, these processes are energetically excluded from the possible excitation processes of He*. Since only the nondissociative ion–ion neutralization process (11) is energetically accessible for the formation of He*, it was concluded to be the excitation source of He*.

The emitting excited He* states formed in each neutralization process (11) and their excitation energies are listed in Table I, together with corresponding data for the $He^+/2e^-$ reactions.[7] The electron affinities of C_6F_5X are also given in the first column of Table I. Figure 3 shows an energy-level diagram of He* and the potential energies of $He^+ + C_6F_5X^-$ at an infinite interparticle distance. The energy levels of He* are shown for those observed in the $He^+/2e^-$ reaction.[7] We have recently found that He* atoms in the $He^+/2e^-$ reaction are excited up to 0.06–1.87 eV below the energy of He^+, and the energy of the highest populated level increases with an increase in the degeneracy of He*.[7] We found here that the highest populated levels of He* in the $He^+/C_6F_5X^-$ reactions are 0.04–1.0 eV below the entrance $He^+ + C_6F_5X^-$ potentials. The highest populated level of He* in the $He^+/C_6F_6^-$ reaction is the $3p\,^1P$ state, with an excitation energy of 23.09 eV. On the other hand, that in the $He^+/C_6F_5X^-$ (X=Cl, CF_3) reactions is the $4d\,^3D$ state with a higher excitation energy of 23.73 eV, though the electron affinities of C_6F_5X (X=Cl, CF_3) are larger than that of C_6F_6. This shows that there is little correlation between the highest populated levels and the electron affinity of C_6F_5X. The lack of the $4d$ state in the $He^+/C_6F_5Br^-$ reaction is explained by the endothermicity of the reaction due to a high electron affinity of C_6F_5Br (see Fig. 3).

B. Electronic-state distributions of He*

The electronic-state distributions of He* in the $He^+/C_6F_5X^-$ reactions were evaluated from the emission intensity of a (u,l) transition of He*, I_{ul}, using the following relation:

$$P_u = A_{ul}N_u \propto \sum_l I_{ul} \propto k_u. \quad (14)$$

Here, P_u is the initial electronic-state distribution, A_{ul} is the Einstein coefficient, N_u is the steady-state distribution, and k_u is the relative formation rate of He*. The normalized N_u

TABLE I. Electronic-state distributions of He* formed by the $He^+/C_6F_5X^-$ (X=F, Cl, Br, CF_3) neutralization in the He afterglow at 300 K, crossing points, and radial distributions of each He* orbital at crossing points.

State Energy (eV)		$3s\,^3S$ 22.72	$3s\,^1S$ 22.92	$3p\,^3P$ 23.01	$3p\,^1P$ 23.09	$3d\,^3D$ 23.07	$3d\,^1D$ 23.07	$4s\,^3S$ 23.59	$4d\,^3D$ 23.73	Other states
	k(obs)	7.9E-1	9.7E-2	1.9E-2	4.7E-3	4.4E-2	4.8E-2			
	k(model A)	9.4E-2	2.9E-2	2.5E-1	8.1E-2	4.1E-1	1.4E-1			
$C_6F_6^-$	k(model B)	1.0	2.1E-3	1.5E-3	4.2E-5	3.9E-4	1.3E-4			
(0.52 eV)[a]	N_u	7.6E-1	1.4E-1	5.5E-2	9.4E-3	1.6E-2	2.0E-2			
This work	R_c(Å)	10.66	12.52	13.59	14.70	14.41	14.41	30.15	42.71	
	$R_c^2R_{nl}^2(R_c)$	9.2E-6	2.4E-7	4.5E-10	4.2E-11	5.4E-13	5.4E-13	1.1E-14	3.6E-28	
	k(obs)	8.5E-1	7.4E-2	1.6E-2	2.0E-3	3.3E-2	2.6E-2	1.3E-3	1.4E-3	
	k(model A)	7.8E-2	2.4E-2	2.0E-1	4.1E-2	6.5E-2	3.3E-1	4.1E-2	1.6E-1	
$C_6F_5Cl^-$	k(model B)	1.0	7.6E-4	2.9E-4	4.5E-6	5.0E-5	1.7E-5	3.0E-14	1.3E-26	
(0.74 eV)	N_u	8.1E-1	1.1E-1	4.5E-2	4.0E-3	1.2E-2	1.1E-2	3.7E-3	1.5E-3	
This work	R_c(Å)	12.74	15.50	17.17	18.98	18.49	18.49	56.05	123.71	
	$R_c^2R_{nl}^2(R_c)$	1.5E-7	5.1E-10	1.9E-13	3.3E-15	5.0E-17	5.0E-17	1.1E-33	7.4E-92	
	k(obs)	9.6E-1		3.8E-2						
	k(model A)	2.8E-1		7.2E-1						
$C_6F_5Br^-$	k(model B)	1.0		7.3E-7						
(1.15 eV)	N_u	8.9E-1		1.1E-1						
This work	R_c(Å)	20.04	27.81	33.69	41.47	39.21	39.21			
	$R_c^2R_{nl}^2(R_c)$	2.8E-14	6.7E-22	4.9E-30	4.3E-38	2.1E-38	2.1E-38			
	k(obs)	9.4E-1		1.0E-2		4.5E-2		1.6E-3	3.5E-3	
	k(model A)	1.0E-1		2.6E-1		4.2E-1		4.8E-2	1.6E-1	
$C_6F_5CF_3^-$	k(model B)	1.0		9.3E-6		6.5E-7		3.4E-28	1.1E-39	
(0.82 eV)	N_u	9.4E-1		3.1E-2		1.8E-2		4.8E-3	3.9E-3	
This work	R_c(Å)	13.72	16.96	18.98	21.23	20.62	20.62	81.53	398.61	
	$R_c^2R_{nl}^2(R_c)$	2.1E-8	2.3E-11	3.3E-15	2.0E-17	3.6E-19	3.6E-19	2.7E-53	≅0	
$2e^-$	k(obs)	2.2E-1	2.2E-2	2.8E-2	1.4E-2	3.4E-1	2.4E-1	4.6E-3	5.3E-2	7.8E-2
Ref. 7	N_u	2.1E-1	3.2E-2	8.1E-2	2.7E-2	1.3E-1	9.9E-2	1.3E-2	5.6E-2	3.5E-1

[a]Electron affinity of C_6F_5X.

and k_u values obtained using known A_{ul} data[27,28] are given in Table I. For comparison, corresponding data for the $He^+/2e^-$ reaction are also given in the last line of Table I. The observed N_u and k_u values were essentially independent of the He gas pressure in the 0.6–2.5 Torr range and the distance between the discharge and the observed region, which was about 10 or 20 cm. This shows that electronic relaxation involving excitation transfer between singlet and triplet states by collisions with buffer He atoms were insignificant under the present experimental conditions.

The N_u distributions can be classified into two groups. One is X=F and Cl, for which both singlet and triplet He* states are populated. The other is X=Br and CF_3, for which only triplet He* states are populated. The ΣN_u(triplet)/ΣN_u(singlet) ratios are 4.9 and 6.8 for X=F and Cl, respectively. Since the ΣN_u(triplet)/ΣN_u(singlet) ratio in the $He^+/2e^-$ reaction is 2.6,[7] the formation of triplet states is much more favored in the $He^+/C_6F_5X^-$ reactions. Both singlet and triplet entrance He^+–$C_6F_5X^-$ surfaces are possible, because He^+ and $C_6F_5X^-$ are doublet. Some trajectory change from singlet He^+–$C_6F_5X^-$ surfaces to triplet He^+–$C_6F_5X^-$ surfaces probably occurs in the $He^+/C_6F_5X^-$ reactions. Such a trajectory change becomes significant for $C_6F_5X^-$ with a heavier X due to a stronger spin-orbit interaction, so that the ΣN_u(triplet)/ΣN_u(singlet) ratio will become large with increasing the mass of X. The N_u values in

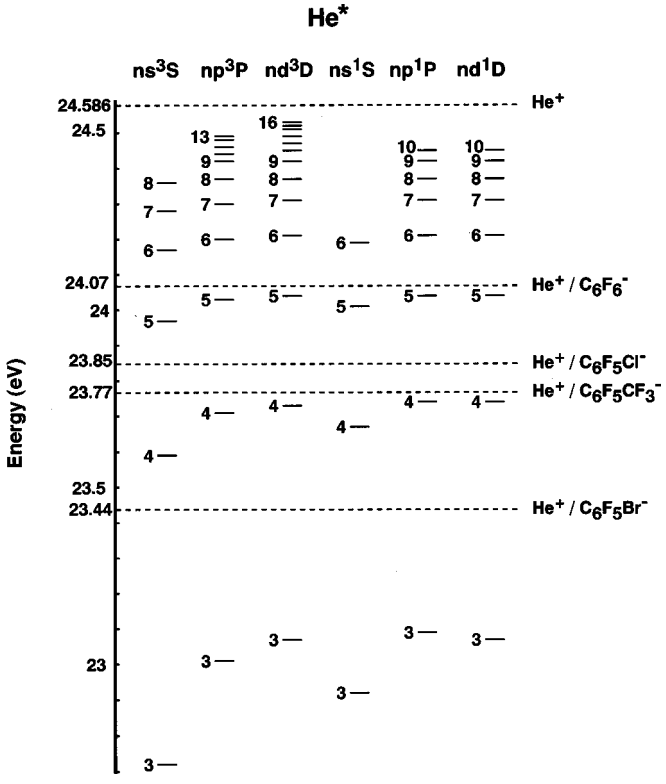

FIG. 3. An energy-level diagram of He* and $He^+ + C_6F_5X^-$. The energy levels of He* are shown for those excited in the $He^+/2e^-$ reaction (Ref. 7).

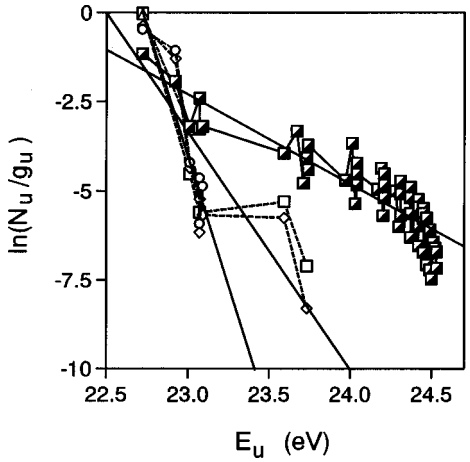

FIG. 4. The dependence of $\ln(N_u/g_u)$ on the excitation energy of He* in the $He^+/C_6F_5X^-$ and $He^+/2e^-$ reactions (Ref. 7) in a He flowing afterglow. ○: $He^+/C_6F_6^-$, ◇: $He^+/C_6F_5Cl^-$, △: $He^+/C_6F_5Br^-$, □: $He^+/C_6F_5CF_3^-$, ◪: $He^+/2e^-$.

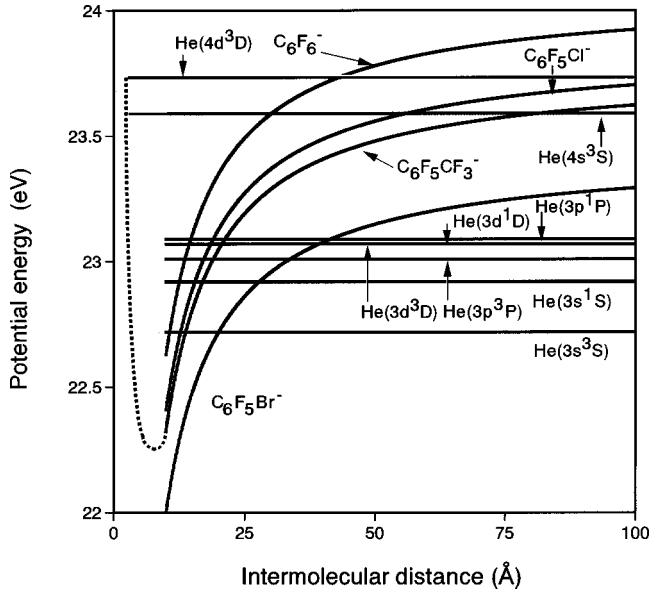

FIG. 5. Entrance $He^+ + C_6F_5X^-$ ion curves and exit $He^* + C_6F_5X$ covalent potentials.

the $He^+/C_6F_5X^-$ reactions decrease more rapidly than those in the $He^+/2e^-$ reaction with increasing excitation energy of He*, and the dependence of N_u on the excitation energy is similar in the energy range of 22.72–23.07 eV. The most favorite product state is the lowest observed He($3s\,^3S$) state, which occupies 76%–94% of the total population.

Assuming a Maxwell–Boltzmann distribution, N_u is given by

$$N_u \propto g_u \exp(-E_u/kT_e), \tag{15}$$

where E_u is the excitation energy of He*. If a plot of $\ln(N_u/g_u)$ vs E_u is linear, then the distribution can be characterized by a Boltzmann electronic temperature (T_e). Of course, this electronic temperature is not equal to any other temperatures (translational, vibrational, and rotational) that would exist in a fully equilibrated system. Figure 4 shows a plot of $\ln(N_u/g_u)$ vs E_u. Assuming a single Boltzmann distribution in each process, Boltzmann electronic temperatures of 0.070, 0.16, 0.090, and 0.19 eV are obtained for X=F, Cl, Br, and CF_3, respectively. It was found that more than 99% of the product He* atoms are formed in the low-lying He($3s,3p,3d$) states below 23.07 eV and their distributions are similar for all four reactions. The electronic-state distribution of He($3s,3p,3d$) in all the four reactions is expressed by a Boltzmann temperature of 0.069 eV, as shown in Fig. 4. When data for the upper He($4s,4d$) states in the $He^+/C_6F_5X^-$ (X=Cl, CF_3) reactions are added to those of the He($3s,3p,3d$) states, the total distribution is expressed by a higher Boltzmann temperature of 0.15 eV, as shown in Fig. 4. These two electronic temperatures are lower than that in the $He^+/2e^-$ reaction (0.40 eV). A major reason for the lower electronic temperatures in the $He^+/C_6F_5X^-$ reactions is lower available energies due to the positive electron affinity of C_6F_5X. The N_u value of the lowest $3s\,^3S$ state is largest among the observed He* states. It increases from 0.076 to 0.94, with increasing the mass of X in the $He^+/C_6F_5X^-$ (X=F, Cl, Br) reactions. A similar tendency was found for the ion–ion neutralization reactions of $NO^+/C_6F_5X^-$ (X=F, Cl, Br) leading to NO($A\,^2\Sigma^+$, $C\,^2\Pi_r, D\,^2\Sigma^+$), where the branching ratio of the lowest NO($A\,^2\Sigma^+$) state increases with increasing the mass of X.[12]

The $He^+/C_6F_5X^-$ reactions proceed through curve crossings between strongly attractive Coulombic $He^+ + C_6F_5X^-$ entrance potentials and flat exit covalent $He^* + C_6F_5X$ potentials, as shown Fig. 5. The crossing points R_c were calculated from the relation

$$R_c = e^2/(\mathrm{IP} - \mathrm{EA}), \tag{16}$$

where IP is the ionization potential of He* and EA is the electron affinity of C_6F_5X. The R_c values for the formation of each He* state were calculated using EA values of C_6F_6 (0.52 eV), C_6F_5Cl (0.74 eV), C_6F_5Br (1.15 eV), and $C_6F_5CF_3$ (0.82 eV).[15–18] The results obtained are given in Table I. Most of the product states are produced via curve crossings at interparticle distances of 11–34 Å. It should be noticed that the R_c values for the formation of the upper He ($4s,4d$) states from the $He^+/C_6F_5X^-$ (X=Cl, CF_3) reactions are unusually large (56–399 Å). According to Landau–Zener theory, the probability of electron transfer falls off rapidly at large R_c because of the rapidly diminishing nonadiabatic coupling matrix elements, and therefore the reaction efficiencies should be vanishingly small. A similar result has recently been found by Španěl and Smith[29] for the formation of NO($A^2\Sigma^+$) from the NO^+/I^- recombination reaction, where the R_c value is unacceptably large (70 Å). They predicted that the electron transfer from I^- to NO^+ occurs in the vicinity of the repulsive potential wall, i.e., at very short internuclear distance where the kinetic energy previously imparted to the ions has been diminished toward zero by retardation. A similar electron transfer at an inner part probably occurs in the $He^+/C_6F_5X^-$ reactions for the formation of the upper He($4s,4d$) states, as shown in Fig. 5 for the case of the $He^+/C_6F_5CF_3^-$ reaction.

The neutralization leading to He* atoms takes place via an electron transfer from a singly occupied molecular orbital

(SOMO) of $C_6F_5X^-$ to a vacant orbital of He^+. According to an ESR study of Symons,[30] an electron is captured by C_6F_5X (X=F, Cl, Br) in solid matrix at 77 K into a σ^* orbital rather than a π^* orbital. They assumed that these anions have nonplanar carbon structures similar to the chair form of cyclohexane. However, later intermediate neglect of differential overlap (INDO) calculations of the geometrical and electronic structures of $C_6F_6^-$ by Shchegoleva *et al.*[31] demonstrated that a planar carbon structure with C–F bonds bent in and out of the plane fits the coupling constants in ESR better. He reported that the extra electron occupies a combination of π^* and σ^* orbitals with a prevailing π^* component. According to recent *ab initio* calculations of $C_6F_6^-$ by Hiraoka *et al.*[32] using the unrestricted Hartree–Fock (UHF) Slater-type orbitals (STO)-3G method, two anions (C_{2v} and D_2 isomers) are formed by an electron attachment to C_6F_6. Energetically, the C_{2v} isomer with a planer carbon ring and out-of-plane C–F bonds is slightly more stable (0.1 kcal/mol by STO-3G and 1.6 kcal/mol by 3-21G) than the D_2 isomer. The electron in the SOMO is localized dominantly on the C_1–F_7 and C_4–F_{10} bonds. According to semiempirical modified neglect of diatomic overlap (MNDO)-UHF calculations by Glidewell,[33] although the lowest unoccupied molecular orbital (LUMO) of C_6F_5X (X=Cl, Br) is a π^* orbital, upon electron capture a reorganization of the orbitals occurs, causing the added electron to reside in a σ^* SOMO strongly localized on the C–X bond. The SOMO density of X=Br at X is higher than that of X=Cl. When we calculated SOMO of $C_6F_5X^-$ (X=F, Cl, Br, CF_3) using the UHF-PM3 method, these anions have planar structures, and an excess electron was dominantly located on the P_z orbital of the C_1 and C_4 carbons in the C–X and C–F bonds. No significant difference in the electron distribution in SOMO of $C_6F_5X^-$ is found, which is consistent with a similar electronic-state distribution of He*. However, the reliability of these semiempirical calculations may be questioned. Therefore, further detailed *ab initio* configuration interaction (CI) calculations with large basis sets will be required to discuss the relationship between molecular structures of $C_6F_5X^-$ and the observed electronic-state distributions.

As discussed above, the equilibrium geometry of $C_6F_6^-$ depends on the theoretical treatment. Both a carbon skeleton distorted to a cyclohexane-like chair and an undistorted carbon skeleton with out-of-plane C–F bonds have been proposed. Anyway, a significant change in the equilibrium structure is expected by the neutralization from $C_6F_6^-$ to C_6F_6. Chen *et al.*[34] estimated that the equilibrium internuclear distance of $C_6F_6^-$ (~1.6 Å) is longer than that of C_6F_6 (~1.4 Å) and the vertical electron affinity is larger than that of the adiabatic one by about 1 eV. Thus, the excess energy released in the neutralization process must be partitioned into not only the relative translational energy due to the Coulombic attractive force but also the vibrational energy of C_6F_6. On the basis of ESR data at 77 K,[30] equilibrium geometries of $C_6F_5X^-$ (X=Cl, Br) are expected to be significantly different from those of neutral molecules. It is therefore reasonable to assume that some part of the excess energy is imparted into the vibrational energy of C_6F_5X (X=Cl, Br), as in the case of C_6F_6.

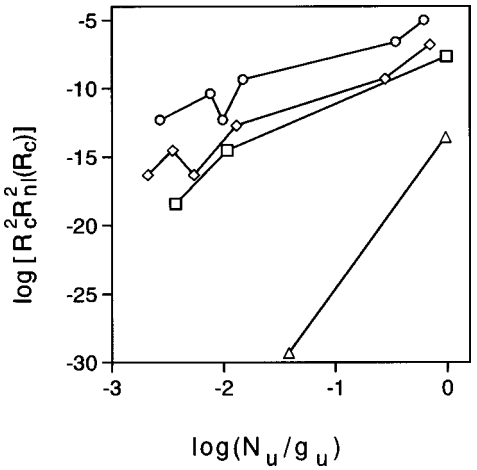

FIG. 6. The dependence of $\log_{10}(N_u/g_u)$ on $\log_{10}[R_c^2R_{nl}^2(R_c)]$. ○: $He^+/C_6F_6^-$, ◇: $He^+/C_6F_5Cl^-$, △: $He^+/C_6F_5Br^-$, □: $He^+/C_6F_5CF_3^-$.

Since the mutual neutralization proceeds through an overlap of SOMO orbital of $C_6F_5X^-$ and a vacant orbital of He^+, the electron density at R_c must be important. In general, radial distribution function, which gives the probability of finding the electron between two spheres of radius R and $R+dR$, is given by $4\pi R^2R_{nl}^2$. The radial distributions of each He* orbital at R_c were calculated using hydrogen-like atomic orbitals. The $R_c^2R_{nl}^2(R_c)$ values are given in Table I. The $R_c^2R_{nl}^2(R_c)$ values are extremely small for the upper He($4s$,$4d$) states having long R_c values of 56–399 Å. This supports our conclusion that the formation of the He($4s$,$4d$) states does not occur via curve crossings at outer parts but they are formed via curve crossings at inner parts. The relationships between the observed $\log_{10}(N_u/g_u)$ values and the $\log_{10}[R_c^2R_{nl}^2(R_c)]$ values for states with $R_c \leqslant 34$ Å are given in Fig. 6. The $\log_{10}(N_u/g_u)$ values increase with increasing radial distribution of electrons for all the four reactions. The increase in the relative population of the lower He* state can be explained by the fact that the overlapping between the SOMO orbital of $C_6F_5X^-$ and a vacant orbital of He^+ increases at a shorter distance. This result led us to conclude that the radial distribution of vacant orbital of He^+ at R_c is an important factor in accessing the N_u distributions in the He^+–$C_6F_5X^-$ reactions.

Since the mutual neutralization reaction proceeds through a strongly attractive potential, He* may be formed via a long-lived (He^+–$C_6F_5X^-$) intermediate, where the excess energy is randomized statistically. Statistical (prior) distributions were calculated in order to examine this prediction. Two statistical models were used for the calculations of the prior distributions,

$$He^+ + C_6F_5X^- \rightarrow [He^+ - C_6F_5X^-] \rightarrow He^* + C_6F_5X. \quad (17)$$

In model A, the $C_6F_5X^-$ anion is assumed to be an atomic ion. On the other hand, all vibrational and rotational degrees of freedom of $C_6F_5X^-$ are included in model B under the rigid-rotor harmonic-oscillator approximation. The final expression for the prior electronic state distribution is given by

$$k(\text{prior}) \propto (2J+1)(E_{\text{excess}} - E_u)^n, \quad (18)$$

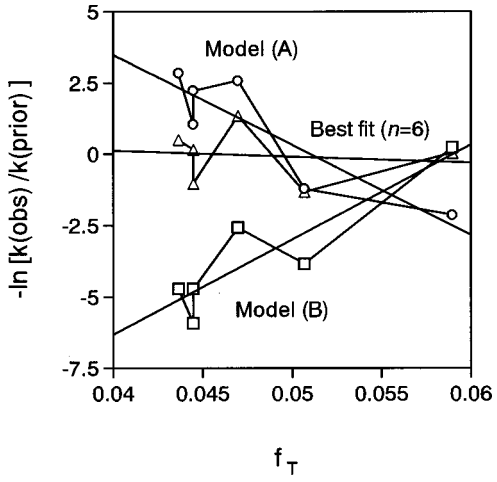

FIG. 7. Surprisal plots of He* produced from the $He^+/C_6F_6^-$ reaction.

where $(2J+1)$ is the statistical weight of an upper state, E_{excess} is the total available energy, which is estimated from the relation $E_{\text{tot}}=\Delta H_0^\circ+3RT$, and $n=1/2$ for model A, and $n=67/2$ for $C_6F_5X^-$ (X=F, Cl, Br) and $n=76/2$ for $C_6F_5CF_3^-$ in model B.[35,36] The prior distributions obtained for the above two models are given in Table I. A significant discrepancy is found between the observed and calculated k values. This shows that both models are inadequate to explain the observed k values. The deviation from the prior distribution has often been represented in the form of a linear surprisal,[35,36]

$$I=-\ln[k(\text{obs})/k(\text{prior})]=\lambda_e f_T+\text{const.} \tag{19}$$

For example, surprisal plots of He* produced from the $He^+/C_6F_6^-$ reaction are shown in Fig. 7. Assuming linear surprisal, the λ_e values of -163.3 and 710.9 were obtained for models A and B, respectively. From similar surprisal analyses, the λ_e values of -122.7 (X=Cl), -346.7 (X=Br), and -315.2 ($X=CF_3$) were obtained for model A, while those of 1827.8 (X=Cl), 904.9 (X=Br), and 352.2 ($X=CF_3$) were obtained for model B. The negative and positive λ_e values for models A and B suggest that the k(obs) values are less and more electronically excited than the k(prior) ones, respectively. When the k(prior) distributions were calculated using various n values, the best fit n values were 6, 5, 4, and 2 for X=F, Cl, Br, and CF_3, respectively, as shown in Fig. 7 for the case of X=F. On the basis of these facts, the excess energies are not partitioned into all vibrational and rotational modes of C_6F_5X, but they are imparted into 2–6 active modes in C_6F_5X, which amount to 5%–45% of the total vibrational and rotational modes. This shows that $[He^+-C_6F_5X^-]$ intermediates have not enough lifetimes to randomize the excess energy completely.

IV. CONCLUDING REMARKS

The electronic-state distributions of He* produced by the $He^+/C_6F_5X^-$ reactions have been determined (Table I). The steady-state populations of He* were expressed by single Boltzmann electronic distributions with effective electronic temperatures of 0.070–0.19 eV. Statistical prior distributions were calculated using two models. In one model, $C_6F_5X^-$ was assumed as an atomic ion, while all vibrational and rotational degrees of freedom in C_6F_5X were considered in the other model. The observed electronic-state distributions were either higher or lower than those predicted from the former and latter models, respectively. It was therefore concluded that the excess energies were partitioned into some specific internal modes of C_6F_5X. A good correlation was found between the observed electronic-state distribution and radial distribution of vacant orbitals of He^+ to which an electron is transferred. In order to obtain more information on the mechanism of ion–ion neutralization processes of He^+ with $C_6F_5X^-$, detailed *ab initio* calculations of molecular orbitals of anions and overlap integrals between SOMO of $C_6F_5X^-$ and vacant orbitals of $He^+(n=3,4)$ will be necessary.

ACKNOWLEDGMENTS

The authors are grateful to Dr. Kazunari Shimokawa and Dr. Seiko Kiyokawa of the Tokyo Metropolitan Industrial Technology Research Institute for their helpful correspondence, and the late Professor Hiroshi Shimamori at Fukui Institute of Technology for his helpful discussion. This work was partially supported by the Mitsubishi Foundation and a Grant-in-Aid for Scientific Research No. 09440201 from the Japanese Ministry of Education, Science, Sports, and Culture.

[1] M. R. Flannery, in *Advances in Atomic, Molecular, and Optical Physics*, edited by B. Bederson and A. Dalgarno (Academic, New York, 1994), Vol. 32, p. 117.
[2] M. Tsuji, *Trends in Physical Chemistry* (Science Information, Trivandrum, India, 1995), Vol. 5, p. 25.
[3] M. Tsuji, K. Kobarai, H. Kouno, H. Obase, and Y. Nishimura, J. Chem. Phys. **94**, 1127 (1991).
[4] M. Tsuji, M. Nakamura, Y. Nishimura, and H. Obase, J. Chem. Phys. **103**, 1413 (1995).
[5] M. Tsuji, M. Nakamura, and Y. Nishimura, Chem. Lett. **1997**, 259.
[6] M. Tsuji, M. Nakamura, Y. Nishimura, and H. Obase, J. Chem. Phys. **108**, 8031 (1998).
[7] M. Tsuji, M. Nakamura, E. Oda, M. Hisano, and Y. Nishimura, Jpn. J. Appl. Phys., Part 1 **37**, 5775 (1998).
[8] M. Tsuji, M. Furusawa, H. Kouno, and Y. Nishimura, J. Chem. Phys. **94**, 4291 (1991).
[9] M. Tsuji, H. Ishimi, M. Nakamura, Y. Nishimura, and H. Obase, J. Chem. Phys. **102**, 2479 (1995).
[10] M. Tsuji, H. Ishimi, Y. Nishimura, and H. Obase, J. Chem. Phys. **102**, 6013 (1995).
[11] M. Tsuji, H. Ishimi, Y. Nishimura, and H. Obase, Int. J. Mass Spectrom. Ion Processes **145**, 165 (1995).
[12] M. Tsuji, H. Ishimi, Y. Nishimura, and H. Obase, J. Chem. Phys. **105**, 2701 (1996).
[13] M. Tsuji, in *Techniques of Chemistry*, edited by J. M. Farrar and W. H. Saunders, Jr. (Wiley, New York, 1988), Vol. 20, p. 489.
[14] Y. Ikezoe, S. Matsuoka, M. Takebe, and A. Viggiano, *Gas Phase Ion-Molecule Reaction Rate Constants through 1986* (Maruzen, Tokyo, 1987).
[15] S. Chowdhury, E. P. Grimsrud, T. Henis, and P. Kebarle, J. Am. Chem. Soc. **108**, 3630 (1986); G. W. Dillow and P. Kebarle, *ibid.* **111**, 5592 (1989).
[16] H. Shimamori, Y. Tatsumi, and T. Sunagawa, J. Chem. Phys. **99**, 7787 (1993); Y. Ninomiya, T. Sunagawa, Y. Tatsumi, and H. Shimamori, Abstract of 27th Annual Meeting of Jpn. Radiation Chem. (1997), 3P23, p. 129.
[17] C. R. Herd, N. G. Adams, and D. Smith, Int. J. Mass Spectrom. Ion Processes **87**, 331 (1989).
[18] F. J. Davis, R. N. Compton, and D. R. Nelson, J. Chem. Phys. **59**, 2324 (1973).

[19] D. Smith, C. V. Doodall, and M. J. Copsey, J. Phys. B **1**, 660 (1968).
[20] D. Smith and I. I. Plumb, J. Phys. D **6**, 196 (1973).
[21] A. R. Striganov and N. S. Sventitskii, *Tables of Spectral Lines of Neutral and Ionized Atoms* (Plenum, New York, 1979).
[22] J. P. Maier, O. Marthaler, M. Mohraz, and R. H. Shiley, Chem. Phys. **47**, 295 (1980).
[23] M. Endoh, M. Tsuji, and Y. Nishimura, Chem. Phys. **82**, 67 (1983).
[24] C. E. Moore, *Atomic Energy Levels*, Natl. Bur. Stand. (U.S.) Circ. 467 (U.S. GPO, Washington D.C., 1949).
[25] S. G. Lias, J. E. Bartmess, J. F. Liebman, J. L. Holmes, R. D. Levin, and W. G. Mallard, J. Phys. Chem. Ref. Data Suppl. **17**, 1 (1988); updated data were obtained from NIST Standard Ref. Database, Number 69, 1997, (http://webbook.nist.gov/chemistry).
[26] K. P. Huber and G. Herzberg, *Molecular Spectra and Molecular Structure, IV. Constants of Diatomic Molecules* (Van Nostrand, New York, 1979).
[27] J. Reader, C. H. Corliss, W. L. Wiese, and G. A. Martin, *Wavelengths and Transition Probabilities for Atoms and Atomic Ions*, NSRDS-NBS 68 (U.S. GPO, Washington D.C., 1981).
[28] C. E. Theodosiou, At. Data Nucl. Data Tables **36**, 97 (1987).
[29] P. Španěl and D. Smith, Chem. Phys. Lett. **258**, 477 (1996).
[30] M. C. R. Symons, J. Chem. Soc., Faraday Trans. 1 **77**, 783 (1981).
[31] L. N. Shchegoleva, I.I. Bilkis, and P. V. Schastnev, Chem. Phys. **82**, 343 (1983).
[32] K. Hiraoka, S. Mizuse, and S. Yamabe, J. Phys. Chem. **94**, 3689 (1990).
[33] C. Glidewell, Chem. Scr. **25**, 145 (1985).
[34] E. C. Chen, E. S. D. Chen, and W. E. Wentworth, J. Chem. Phys. **100**, 6981 (1994).
[35] R. D. Levine, Annu. Rev. Phys. Chem. **29**, 59 (1978).
[36] R. D. Levine and J. L. Kinsey, in *Atom-Molecule Collision Theory*, edited by R. B. Bernstein (Plenum, New York, 1979) p. 693.